Influence of point defects on the thermal conductivity in FeSi

Robin Stern,[1] Tao Wang,[1] Jesús Carrete,[2] Natalio Mingo,[3] and Georg K. H. Madsen[2,*]
[1]*AMS, ICAMS, Ruhr-Universität Bochum, 44801 Bochum, Germany*
[2]*Institute of Materials Chemistry, TU Wien, A-1060 Vienna, Austria*
[3]*LITEN, CEA-Grenoble, 17 rue des Martyrs, 38054 Grenoble Cedex 9, France*

(Received 28 September 2017; revised manuscript received 15 December 2017; published 7 May 2018)

The unique transport properties of B20 FeSi have been investigated for decades. The progress in theoretical calculations allows the explanation and prediction of more and more of such properties. In this paper we investigate the lattice thermal conductivity of FeSi. Calculation for pristine FeSi severely overestimates the lattice thermal conductivity compared to experiment. We point out that the defect concentration can be considerably larger than indicated by the Hall coefficient. The defect formation energies are calculated and it is found that a substantial amount of iron vacancies can form at thermal equilibrium. These will lead to an increased phonon scattering. To explain the thermal conductivity of FeSi, we consider phonon-phonon, isotope, and phonon-defect scattering to assess possible scattering mechanisms. The calculated thermal conductivities indicate that phonon-defect scattering is important in order to explain the reported experimental values.

DOI: 10.1103/PhysRevB.97.195201

I. INTRODUCTION

Cubic FeSi is a material where a number of properties exhibit unique temperature dependencies. One example is the closing of the narrow band gap at elevated temperatures, such that FeSi becomes metallic [1–6]. Further examples are the magnetic susceptibility, which tends to zero at low temperatures but follows a Curie-Weiss law for high temperatures [7] and the Seebeck coefficient, which peaks and reaches values up to 1200 μV/K at $T < 50$ K [8]. The unusual property vs temperature dependence has been discussed in terms of the thermal disorder of the atoms [9,10] and in terms of effects beyond the Kohn-Sham density functional theory (KS-DFT) description of the electronic structure [11,12]. We recently studied [10] the anomalous 14% downward shift of the acoustic phonon peak that occurs when the temperature of FeSi is raised above 750 K [13]. The effect, which is beyond the expected phonon softening, can be explained within KS-DFT if thermal expansion combined with thermal disorder of the atoms is taken into account [10].

In the present work we focus on the lattice thermal conductivity, κ_ℓ, of FeSi. Considering how KS-DFT seems able to describe the phonon properties of FeSi [10], it would be interesting to see whether the same conclusion applies to the lattice thermal conductivity. Understanding the thermal conductivity of FeSi is a challenging task where phonon-phonon, electron-phonon, as well as phonon-defect interactions, will influence the κ_ℓ of FeSi differently. Experimental data on the κ of FeSi are limited. Buschinger [14], Ou-Yang [15], and Sales *et al.* [8] report values up to 300 K and 200 K, respectively, where phonon anharmonicity is significant. Interestingly, the measured thermal conductivities show considerable discrepancies at low temperatures. Both Buschinger and Sales *et al.* performed measurements on polycrystalline and single-crystal samples and found that the κ of polycrystalline FeSi at 50–70 K is almost double that of the single crystal [8,14]. This is unusual, because polycrystalline materials usually exhibit larger grain-boundary scattering than single crystals. Sales *et al.* attribute this fact to electron-phonon scattering [8]. While measured Hall coefficients would indicate that the defect concentration is also larger in the single-crystal sample, point-defect scattering is ruled out as a possible source of the inverted thermal conductivity due to the overall low carrier concentration [8].

The aim of the present paper is to show that the point-defect concentration can be larger than what would be estimated from the Hall coefficient. Consequently, it can play an important role in lowering the thermal conductivity, as a complementary or alternative mechanism to the electron-phonon coupling. Predictive evaluation of κ_ℓ in the presence of defects that can be comparable with experimental observations is possible thanks to a recently developed *ab initio* Green's function approach [16–18]. The presence of defects can have a large influence on phonon scattering and thus lower the thermal conductivity. We identify the iron vacancy as the most prominent intrinsic defect in FeSi by calculating the defect formation energies. We calculate the phonon-defect scattering rates and the resulting concentration-dependent lattice thermal conductivity of defect-laden FeSi and show that defect concentrations around $c_{\text{def}} = 0.5$–1 % are enough to substantially lower the thermal conductivity and achieve a better agreement with experiment.

II. METHODS

To calculate the thermal conductivity the linearized Boltzmann transport equation in the relaxation time approximation

*georg.madsen@tuwien.ac.at

is used.

$$\kappa_l = \frac{1}{3}\sum_j \int \frac{d\mathbf{q}}{(2\pi)^3} C_{j\mathbf{q}} v_{j\mathbf{q}}^2 \tau_{j\mathbf{q}}, \quad (1)$$

where $j\mathbf{q}$ represent the phonon branch and wave vector, $C_{j\mathbf{q}}$ is the mode contribution to the volumetric heat capacity and $v_{j\mathbf{q}}$ the phonon group velocity. The total scattering rate can be calculated using Matthiessen's rule

$$\frac{1}{\tau_{j\mathbf{q}}} = \frac{1}{\tau_{j\mathbf{q}}^{3p}} + \frac{1}{\tau_{j\mathbf{q}}^{iso}} + \frac{1}{\tau_{j\mathbf{q}}^{def}}. \quad (2)$$

The anharmonic scattering rate, $(\tau_{j\mathbf{q}}^{3p})^{-1}$, is obtained from the second- and third-order interatomic force constants (IFCs) [19]. The harmonic and anharmonic IFCs of the unperturbed system were calculated in a $3 \times 3 \times 3$ and $2 \times 2 \times 2$ supercell with $3 \times 3 \times 3$ and $5 \times 5 \times 5$ k-point meshes, respectively. Thermal conductivities including three-phonon and isotope scattering were calculated using the almaBTE code [20]. The results were compared to those obtained from the PHONO3PY code [21] and a very good agreement was obtained.

The IFCs are obtained by expanding the interatomic forces around the atomic equilibrium positions up to third order

$$F_{\alpha_1}^m = -\sum_{n\alpha_2} \phi_{\alpha_1\alpha_2}^{mn} u_{\alpha_2}^n - \frac{1}{2}\sum_{nh\alpha_2\alpha_3} \psi_{\alpha_1\alpha_2\alpha_3}^{mnh} u_{\alpha_2}^n u_{\alpha_3}^h. \quad (3)$$

Similar to our earlier work on the harmonic IFCs [10] we recast this as

$$\mathbf{F}_m = -\sum_n \tilde{u}_n \phi^{mn} - \frac{1}{2}\sum_{nh} \tilde{u}_{nh} \psi^{mnh}, \quad (4)$$

where $\tilde{u}$ are 3×9 and 3×27 dimensional matrices, respectively. ϕ^{mn} and ψ^{mnh} are the independent IFCs written as vectors and $\tilde{u}$ represent symmetry-dependent linear combinations of the displacements. m, n, and h are atomic indices and α are Cartesian coordinates.

The forces on the atoms are the result of the displacements of all atoms in the supercell. The main advantage of obtaining the IFCs by inverting Eq. (4) is that the forces on the atoms can be obtained by displacing all atoms in the supercell simultaneously. At thermal equilibrium, the probability of a set of displacements is solely a function of temperature. Thereby temperature-dependent effective IFCs and temperature-dependent phonon properties can be obtained [10,22]. Compared to 10 K, a 3% softening of the main acoustic peak in FeSi is experimentally observed at 200 K [13]. Using the method of temperature-dependent effective IFCs we have previously reproduced the phonon softening in FeSi, and shown that both thermal expansion and thermal disorder contribute [10]. To investigate the role of thermal disorder on the lattice thermal conductivity we consider configurations, where all atoms are displaced by a finite amount in random directions with the amplitude of 0.015 Å at the calculated unit cell volume of 88.1 Å^3. The convergence of the obtained third-order IFCs and the resulting thermal conductivity was monitored with respect to the number of stochastic displacements. Calculating forces for 1100 configurations of finite stochastic displacements gives a κ_ℓ at 200 K that is 24 W m^{-1}K^{-1}. Using 1600 and 1800 configurations we obtain a converged value of 25 W m^{-1}K^{-1}. We have further calculated the IFCs and thermal conductivity using standard sequential displacements [19], where the second- and third-order force are calculated by sequentially displacing the atoms one at a time or in pairs, respectively. Hereby a $\kappa_\ell = 21$ W m^{-1}K^{-1} is obtained. As a phonon softening will reduce the average phonon velocities, Eq. (1), it is at first sight surprising that the effective IFCs lead to a higher lattice thermal conductivity. However, the phonon softening is an indication of weaker interatomic interactions, which will be reflected in both lower second-order, ϕ and lower third-order, ψ, IFCs. While the lower second-order IFCs lead to the observed phonon softening, and consequently lower phonon velocities, the lower third-order IFCs will lead to lower scattering rates and enhanced κ_ℓ. To investigate a possible role of thermal expansion, we furthermore calculated κ_ℓ at the experimental low-temperature volume (89.6 Å^3). The volume difference exceeds the 200 K volume expansion, which amount to only 0.2 Å^3 [23]. Using 1800 configurations we obtain a converged value of 25 W m^{-1}K^{-1}, thereby ruling out an influence of thermal expansion at least up to 300 K.

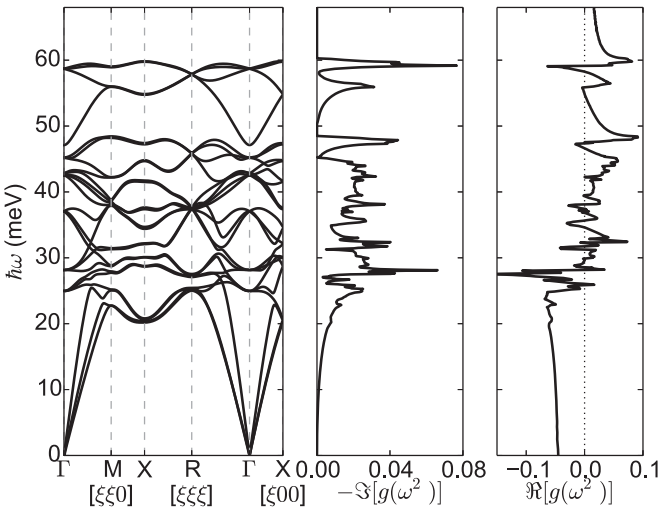

FIG. 1. Band structure, imaginary and real parts of the Green's function computed using the three-dimensional (3D) tetrahedron method as implemented in almaBTE [20] with a $22 \times 22 \times 22$ sampling grid. Second-order IFCs of defect-free FeSi are obtained with a supercell size of $3 \times 3 \times 3$.

To consider phonon-defect scattering rates, we take the perturbation of the IFCs into account using a Green's function approach [24], where $\tau_{j\mathbf{q}}^{-1}$ is given as

$$\frac{1}{\tau_{j\mathbf{q}}^{def}} = -\frac{c_{def} V_{uc}}{\omega_{i\mathbf{q}}} \Im\left\{\langle j\mathbf{q}|\left(\mathbf{I} - \mathbf{V}\mathbf{g}^+\right)^{-1}\mathbf{V}|j\mathbf{q}\rangle\right\}, \quad (5)$$

where c_{def} is the volumetric concentration of the point defects, V_{uc} the volume of the unit cell, and ω the angular frequency of phonons. $\mathbf{g}^+$ is the retarded Green's function of the unperturbed crystal and $\mathbf{V}$ the perturbation matrix. The Green's function, Fig. 1, used in Eq. (5) is computed using the tetrahedron method as implemented in the almaBTE code [20]. For the iron vacancy considered here, $\mathbf{V}$ will be due to the perturbation of the harmonic IFCs.

We calculated the defect formation energies of the intrinsic defects using the supercell approach within DFT [25]. The defect formation energy is given by

$$E_{D^{(q)}}(\mu_e) = E_{f,D^{(q)}} - \sum_\alpha n_\alpha \Delta\mu_\alpha + q\mu_e, \quad (6)$$

where $E_{f,D^{(q)}}$ is the defect formation energy with respect to the reference states

$$E_{f,D^{(q)}} = E_D^{(q)} - E_{\text{bulk}} - \sum_\alpha n_\alpha E_\alpha. \quad (7)$$

The energy to exchange n atoms of kind α with the reservoir is captured in the chemical potentials $\Delta\mu_\alpha$. Furthermore, the defect formation energy depends on the charge state of the defect and the electron chemical potential μ_e. In the binary system of FeSi we first determine the allowed chemical potentials corresponding to Fe- and Si-rich growth conditions. More information on the computational procedure for calculating the defect formation energies and the applied corrections can be found in Ref. [26].

We performed all calculations using the DFT code VASP [27] and the Perdew-Burke-Ernzerhof exchange correlation functional [28]. We relaxed the atomic positions and volume of the unit cell until the energy was converged up to 10^{-8} eV per unit cell, which also minimized the forces in the cell. The defect formation energies were calculated in a $3 \times 3 \times 3$ cubic supercell with 216 atoms to avoid defect-defect interactions and a $4 \times 4 \times 4$ k-point mesh.

III. RESULTS AND DISCUSSION

The thermal conductivity of pristine B20 FeSi from five independent calculations with different mesh sizes are shown in Fig. 2. A q-point mesh of $20 \times 20 \times 20$ can fulfill the convergence requirements of both scattering rate τ^{-1} and thermal conductivity κ_ℓ for $T > 40$ K. The calculated thermal conductivity is also compared to experiment [8,15] in Fig. 2.

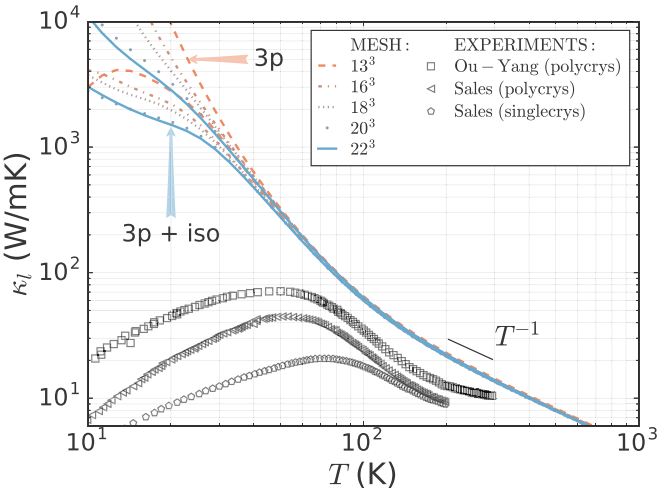

FIG. 2. Thermal conductivity of pure FeSi, where only three-phonon scattering was considered in Eq. (2), and natural FeSi, where three-phonon and isotope scattering were considered in Eq. (2), computed using the single-mode relaxation-time approximation as implemented in almaBTE [20].

Experimentally the lattice thermal conductivity at 200 K is found in a relatively narrow range between 9–12 W m^{-1}K^{-1}. Our calculation, taking only phonon-phonon and isotope scattering into account, gives a $\kappa_\ell = 21$ W m^{-1}K^{-1}, thus clearly overestimating the thermal conductivity. The electronic contribution, κ_e, was subtracted from the experimental κ by applying the Wiedemann-Franz law using a Lorentz number of $L = 2.44 \times 10^{-8}$ WΩK^{-2}. The correction however only amounts to about $\kappa_e \approx 1$ W m^{-1}K^{-1} at 200 K and even less for lower temperatures. Therefore, the discrepancy between the calculated and measured κ_ℓ cannot be attributed to uncertainty in the value of κ_e.

The disagreement between experiment and theory is somewhat surprising as the inclusion of phonon-phonon and isotope scattering has proven highly reliable for the calculation of κ_ℓ in semiconductors [29–32]. In this context, it is notable that a similar poor agreement between theory and experiment has been found for $FeSb_2$ [33], a compound that shows several features which resemble those observed in FeSi [34]. The disagreement would indicate that further scattering mechanisms, in addition to three-phonon and isotope scattering, are important. Electron-phonon coupling has been used to explain the unusual κ in the 50–70 K temperature range, where the polycrystalline κ is almost double that of the single-crystal sample [8]. However, both the two measurement series by Sales and the two by Buschinger *et al.*, which disagree widely at low temperatures, agree well at 200 K [8,14]. It would thus seem that if electron-phonon coupling plays an important role at 50–70 K, other mechanisms must contribute to lowering κ_ℓ at temperatures above 200 K. We have two main reasons for suspecting point-defect scattering of phonons to play an important role in lowering κ_ℓ. First, it has recently been shown how the order-of-magnitude reduction of lattice thermal conductivity in doped 3C-SiC in the same temperature range can be explained by point-defect scattering [35]. Second, point defects occur in thermodynamic equilibrium in any material due to configurational entropy and the defect concentration in semiconductors can be orders of magnitudes larger than indicated by the Hall coefficients. Uncharged defects and, more importantly, compensating electron donor and acceptor defects can occur even for defects with the same chemical identity. One example of this is in Bi_2S_3, where the simultaneous presence of $Ge_{Bi}^{(+1)}$ and $Ge_{Bi}^{(-1)}$ prohibits Ge doping [36].

To find the most stable defects, we calculated the defect formation energies of the intrinsic defects in FeSi. The results are shown in Table I. The defect formation energies were calculated under both Si- and Fe-rich conditions, representing the extrema of the chemical potential domain in which a stable B20 structure is formed. The two types of defects introducing the largest structural distortion in the crystal structure are expected to be interstitial defects and vacancies. The intrinsic interstitial defects have an especially high formation energy, Table I, leading to a negligible concentration of this type of defect. We therefore do not expect this type of defect to have a significant impact on the lattice thermal conductivity. On the other hand, the Fe vacancy, $\square_{Fe}$, has very low defect formation energies, especially under Si-rich growth conditions. The $\square_{Fe}$ defect leads to a substantial relaxation towards the vacancy of four of the seven surrounding Si atoms, Fig. 3. With a growth temperature of 1300 K [8] even a $E_{f,\square_{Fe}} \approx 0.4$ eV

TABLE I. Defect formation energies of intrinsic defects in FeSi at the valence band maximum at charge states between −1 and 1. The vacancy $\square_{Fe}$ has the lowest formation energy in Si- and Fe-rich growth conditions.

	Si-rich (eV)			Fe-rich (eV)		
Defect	−1	0	1	−1	0	1
$\square_{Fe}$	0.24	0.16	0.15	0.43	0.35	0.35
Si_{Fe}	1.03	0.88	0.78	1.41	1.26	1.16
$\square_{Si}$	3.06	2.92	2.89	2.87	2.73	2.70
Fe_{Si}	3.19	3.03	2.98	2.81	2.64	2.60
Si_{Int}	5.35	5.19	5.11	5.54	5.39	5.30
Fe_{Int}	5.98	5.84	5.76	5.79	5.65	5.57

means that a simple Boltzmann distribution would predict a defect concentration of approximately 3%. While this value is not necessarily an accurate estimation of the actual defect concentration in the measured FeSi samples, it is probable that the defect concentration can be substantially higher than the estimation based on the Hall coefficient. That the Hall coefficient is not necessarily a good measure of the actual defect is further underlined by the fact that the $\square_{Fe}^{(+1)}$ and $\square_{Fe}^{(-1)}$ charged defects, regardless of the growth conditions, are very close in energy. This in turn will lead to similar concentrations of $\square_{Fe}^{(+1)}$ and $\square_{Fe}^{(-1)}$ and a cancellation of their contribution to the number of carriers in the system. Figure 4 shows the scattering rates due to isotope scattering, phonon-phonon scattering at 200 K, and $\square_{Fe}$ defects at a low concentration of $c_{def} = 3 \times 10^{18}$ cm^{-3}. We have not separately studied the scattering from the charged $\square_{Fe}$ defects as their local relaxations, in accordance with the expectation that the additional charge FeSi will be delocalized, are very similar to that of the noncharged defect, Fig. 3.

The scattering rates due to defects will scale with the defect concentration, Eq. (5), and Fig. 4 confirms the impression from earlier work [16,35] that vacancies induce a large perturbation of the IFCs and subsequent substantial phonon scattering. The mass-disorder and point-defect scattering rates show the expected ω^4 trends for Rayleigh scattering. We do not find a resonance at low frequencies as in earlier work [35], but nonetheless the scattering from $\square_{Fe}$ will start to become important at 200 K at a defect concentration around $c_{def} \approx 10^{19}$ cm^{-3}.

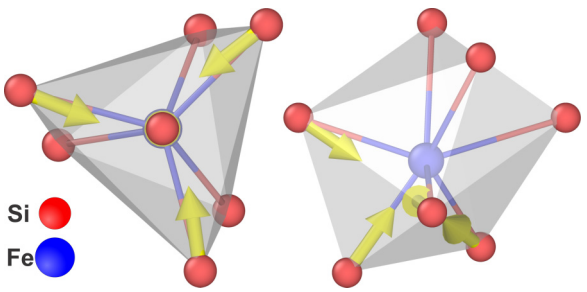

FIG. 3. Local coordination of the Fe atom in FeSi viewed along the [111] (left) and [101] directions. The arrows indicate the direction and magnitude of the local relaxations upon formation of a $\square_{Fe}$ defect.

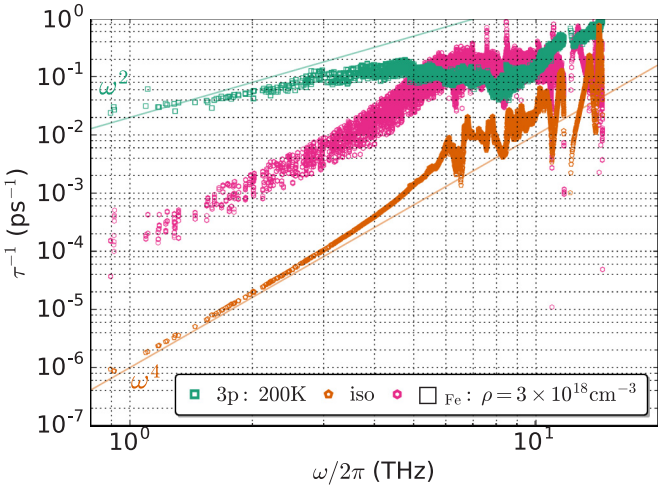

FIG. 4. Multiple phonon scattering rates present in FeSi. For acoustic phonons with long wavelengths $1/\tau^{iso} \propto \omega^4$ for phonon-isotope scattering and $1/\tau^{\square_{Fe}} \propto \omega^4$ for phonon-vacancy scattering.

Figure 5 explores the possibility of explaining the lowered thermal conductivity of FeSi as originating from defect scattering. It is seen that a significant lowering of the lattice thermal conductivity happens at an onset of defect concentration around $c_{def} \approx 0.1\%$ corresponding $c_{def} \approx 5 \times 10^{19}$ cm^{-3}, which is the same order of magnitude as the Hall-coefficient-based estimation [8]. However, the dominating iron-vacancy defect $\square_{Fe}$ is partly noncharged (non-carrier-inducing). Furthermore, the positively charged defect will partly be compensated by the negative. The defect concentration can be thus significantly higher than the Hall-coefficient-based estimation. At a defect concentration $c_{def} \approx 1\%$, corresponding $c_{def} \approx 5 \times 10^{20}$ cm^{-3}, the lattice thermal conductivity is predicted to be approximately 14 Wm^{-1}K^{-1}, in reasonable agreement with the experimental data. As argued above, a defect concentration of $c_{def} \approx 1\%$ is not improbable considering the defect formation energies of the iron vacancy.

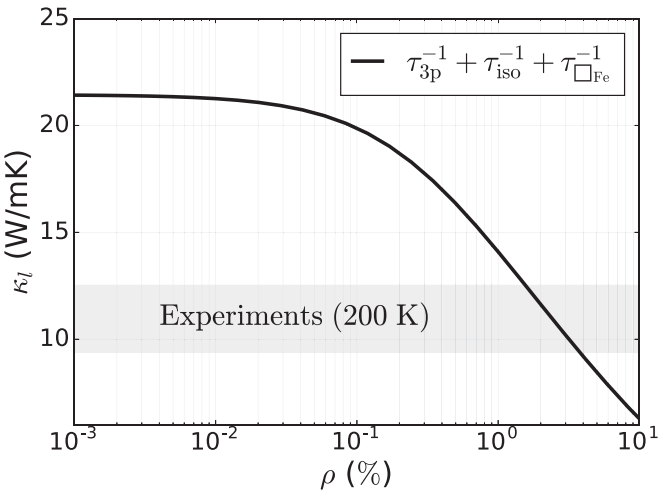

FIG. 5. Thermal conductivity of FeSi at 200 K as a function of Fe vacancy concentration.

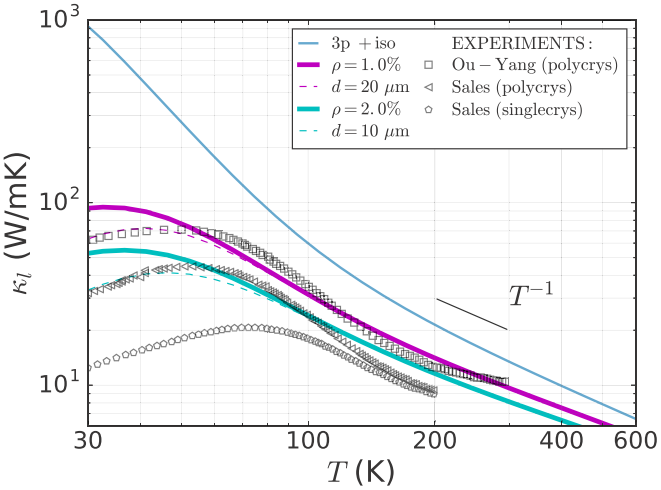

FIG. 6. Thermal conductivity of FeSi as a function of temperature at different vacancy concentrations. Experimental values taken from Refs. [8,15].

It is important to emphasize that we do not rule out electron-phonon scattering or other additional scattering mechanisms. Figure 6 shows how a defect concentration of around 1% can reasonably explain the high-temperature data of Ou-Yang *et al.* [15]. If we include a simple diffuse scattering term for grain boundary scattering

$$\frac{1}{\tau_{j\mathbf{q}}^{\mathrm{gb}}} = \frac{|v_{j\mathbf{q}}|}{L}, \tag{8}$$

where $|v_{j\mathbf{q}}|$ is the norm of the phonon group velocity for phonon mode $j\mathbf{q}$ and L is the grain size, we obtain a good agreement with experiment also at low temperatures employing a rather long $L = 20\ \mu$m. A similar model would require an unrealistically large defect concentration of about 4% to explain the experimental data by Sales *et al.* between 150–200 K. Such a model would at the same time strongly underestimate the thermal conductivity obtained at low temperatures for the polycrystalline sample. The main idea is that we believe point-defect scattering, in addition to other scattering mechanisms, to play a significant role in explaining the thermal conductivity of FeSi. In this context, and considering the temperature dependence and magnitude of the Seebeck coefficient in FeSi [8], it is interesting to note that point defects have also been related to the colossal Seebeck coefficient observed in $FeSb_2$ [37].

IV. CONCLUSION

We calculated the thermal conductivity of B20 FeSi and compared the results to experimental values. We find that anharmonic phonon-phonon scattering and isotope scattering are not sufficient to explain the experimentally measured thermal conductivities. Instead, additional scattering mechanisms have to be taken into account to achieve a reasonable agreement between theory and experiment. While we are not ruling out electron-phonon scattering, we find that the $\square_{\mathrm{Fe}}$ defect has a particularly low formation energy. Phonon-defect scattering due to realistic levels of defect concentrations will significantly lower the thermal conductivity, in good agreement with high-temperature thermal conductivity measurements of FeSi.

ACKNOWLEDGMENTS

We acknowledge support from M-era.net through the ICETS project (DFG: MA 5487/4-1) and the EU Horizon 2020 Grant No. 645776 (ALMA).

[1] Z. Schlesinger, Z. Fisk, H.-T. Zhang, M. B. Maple, J. F. DiTusa, and G. Aeppli, Phys. Rev. Lett. **71**, 1748 (1993).
[2] A. Chainani, T. Yokoya, T. Morimoto, T. Takahashi, S. Yoshii, and M. Kasaya, Phys. Rev. B **50**, 8915 (1994).
[3] T. Saitoh, A. Sekiyama, T. Mizokawa, A. Fujimori, K. Ito, H. Nakamura, and M. Shiga, Solid State Commun. **95**, 307 (1995).
[4] K. Breuer, S. Messerli, D. Purdie, M. Garnier, M. Hengsberger, Y. Baer, and M. Mihalik, Phys. Rev. B **56**, R7061(R) (1997).
[5] S. Paschen, E. Felder, M. A. Chernikov, L. Degiorgi, H. Schwer, H. R. Ott, D. P. Young, J. L. Sarrao, and Z. Fisk, Phys. Rev. B **56**, 12916 (1997).
[6] K. Ishizaka, T. Kiss, T. Shimojima, T. Yokoya, T. Togashi, S. Watanabe, C. Q. Zhang, C. T. Chen, Y. Onose, Y. Tokura *et al.*, Phys. Rev. B **72**, 233202 (2005).
[7] V. Jaccarino, G. K. Wertheim, J. H. Wernick, L. R. Walker, and S. Arajs, Phys. Rev. **160**, 476 (1967).
[8] B. C. Sales, O. Delaire, M. A. McGuire, and A. F. May, Phys. Rev. B **83**, 125209 (2011).
[9] T. Jarlborg, Phys. Lett. A **236**, 143 (1997).
[10] R. Stern and G. K. H. Madsen, Phys. Rev. B **94**, 144304 (2016).
[11] J. Kuneš and V. I. Anisimov, Phys. Rev. B **78**, 033109 (2008).
[12] J. M. Tomczak, K. Haule, and G. Kotliar, Proc. Nat. Acad. Sci. USA **109**, 3243 (2012).
[13] O. Delaire, K. Marty, M. B. Stone, P. R. C. Kent, M. S. Lucas, D. L. Abernathy, D. Mandrus, and B. C. Sales, Proc. Nat. Acad. Sci. USA **108**, 4725 (2011).
[14] B. Buschinger, C. Geibel, F. Steglich, D. Mandrus, D. Young, J. L. Sarrao, and Z. Fisk, Physica B: Condens. Matter **230-232**, 784 (1997).
[15] T. Ou-Yang, Y. Zhuang, B. Ramachandran, W. Chen, G. Shu, C. Hu, F. Chou, and Y. Kuo, J. Alloys Compd. **702**, 92 (2017).
[16] N. A. Katcho, J. Carrete, W. Li, and N. Mingo, Phys. Rev. B **90**, 094117 (2014).
[17] A. Katre, J. Carrete, and N. Mingo, J. Mater. Chem. A **4**, 15940 (2016).
[18] T. Wang, J. Carrete, A. van Roekeghem, N. Mingo, and G. K. H. Madsen, Phys. Rev. B **95**, 245304 (2017).
[19] W. Li, J. Carrete, N. A. Katcho, and N. Mingo, Comput. Phys. Commun. **185**, 1747 (2014).
[20] J. Carrete, B. Vermeersch, A. Katre, A. van Roekeghem, T. Wang, G. K. H. Madsen, and N. Mingo, Comput. Phys. Commun. **220**, 351 (2017).
[21] A. Togo, L. Chaput, and I. Tanaka, Phys. Rev. B **91**, 094306 (2015).
[22] O. Hellman, I. A. Abrikosov, and S. I. Simak, Phys. Rev. B **84**, 180301 (2011).

[23] L. Vočadlo, S. K. Knight, D. G. Price, and G. I. Wood, Phys. Chem. Miner. **29**, 132 (2002).
[24] N. Mingo, K. Esfarjani, D. A. Broido, and D. A. Stewart, Phys. Rev. B **81**, 045408 (2010).
[25] C. Freysoldt, B. Grabowski, T. Hickel, J. Neugebauer, G. Kresse, A. Janotti, and C. G. Van de Walle, Rev. Mod. Phys. **86**, 253 (2014).
[26] R. Stern, B. Dongre, and G. K. H. Madsen, Nanotechnol. **27**, 334002 (2016).
[27] G. Kresse and J. Furthmüller, Phys. Rev. B **54**, 11169 (1996).
[28] J. P. Perdew, K. Burke, and M. Ernzerhof, Phys. Rev. Lett. **77**, 3865 (1996).
[29] D. A. Broido, M. Malorny, G. Birner, N. Mingo, and D. A. Stewart, Appl. Phys. Lett. **91**, 231922 (2007).
[30] A. Ward, D. A. Broido, D. A. Stewart, and G. Deinzer, Phys. Rev. B **80**, 125203 (2009).
[31] W. Li and N. Mingo, J. Appl. Phys. **114**, 183505 (2013).
[32] A. Katre, A. Togo, I. Tanaka, and G. K. H. Madsen, J. Appl. Phys. **117**, 045102 (2015).
[33] B. Liao, S. Lee, K. Esfarjani, and G. Chen, Phys. Rev. B **89**, 035108 (2014).
[34] A. Bentien, S. Johnsen, G. K. H. Madsen, B. B. Iversen, and F. Steglich, Europhys. Lett. **80**, 17008 (2007).
[35] A. Katre, J. Carrete, B. Dongre, G. K. H. Madsen, and N. Mingo, Phys. Rev. Lett. **119**, 075902 (2017).
[36] R. Chmielowski, D. Péré, C. Bera, I. Opahle, W. Xie, S. Jacob, F. Capet, P. Roussel, A. Weidenkaff, G. K. H. Madsen *et al.*, J. Appl. Phys. **117**, 125103 (2015).
[37] M. Battiato, J. M. Tomczak, Z. Zhong, and K. Held, Phys. Rev. Lett. **114**, 236603 (2015).